

RIGA TECHNICAL UNIVERSITY

Faculty of Civil Engineering
Institute of Transportation Engineering

Andris Freimanis

Doctoral Student of the Study Programme “Civil Engineering”

**CRACK DEVELOPMENT ASSESSMENT USING
MODAL ANALYSIS IN PERIDYNAMIC THEORY**

Summary of the Doctoral Thesis

Scientific supervisor
Professor Dr. sc. ing.
AINĀRS PAEGLĪTIS

RTU Press
Riga 2019

Freimanis, A. Crack Development Assessment Using Modal Analysis in Peridynamic Theory. Summary of the Doctoral Thesis. Riga: RTU Press, 2019. 28 p.

Published in accordance with the decision of the Promotion Council P-06 of August 20, 2019, Minutes No. 3-2019.

ISBN 978-9934-22-384-6 (print)
978-9934-22-385-3 (pdf)

DOCTORAL THESIS PROPOSED TO RIGA TECHNICAL UNIVERSITY FOR THE PROMOTION TO THE SCIENTIFIC DEGREE OF DOCTOR OF ENGINEERING SCIENCES

To be granted the scientific degree of Doctor of Engineering Sciences, the present Doctoral Thesis has been submitted for the defence at the open meeting of RTU Promotion Council on 29 November 2019 at the Faculty of Civil Engineering of Riga Technical University, 6B Kipsalas Street , Room 422.

OFFICIAL REVIEWERS

Dr. sc. ing. Sandris Ručevskis
Riga Technical University

Professor Dr. sc. ing. Jānis Andersons
University of Latvia, Latvia

Professor Dr. sc. ing. Darius Bačinskas
Vilnius Gediminas Technical University, Lithuania

DECLARATION OF ACADEMIC INTEGRITY

I hereby declare that the Doctoral Thesis submitted for the review to Riga Technical University for the promotion to the scientific degree of Doctor of Engineering Sciences is my own. I confirm that this Doctoral Thesis had not been submitted to any other university for the promotion to a scientific degree.

Andris Freimanis

Date:

The Doctoral Thesis has been written in English. It consists of Introduction; 6 chapters; Conclusions; 54 figures; 30 tables; 2 appendices; the total number of pages is 114. The Bibliography contains 120 titles.

CONTENTS

1	Introduction	5
1.1	Novelty and Motivation	5
1.2	Aim and Scope	6
1.3	Tasks of the Thesis	6
1.4	Practical Value of the Thesis.....	7
1.5	Arguments for the Defense of the Thesis.....	7
1.6	List of Attended Conferences.....	7
1.7	List of Publications.....	8
2	Theory background.....	9
2.1	Peridynamic Theory	9
2.2	Linear Algebra and Modal Analysis	10
3	Computational implementation and optimization	12
3.1	Peridynamic Implementation	12
	Modal Solver	12
	Peridynamic Model	13
3.2	Finite-Element Implementation.....	13
3.3	Solver Parameter Optimization	14
4	Specimen manufacturing and experimental setup	16
5	Verification and validation of peridynamic modal analysis	18
	Verification and Validation of the PD Modal Frequencies.....	18
	Frequency Shift	19
	Verification of PD Mode Shapes	20
	Validation of the PD Mode Shapes	21
6	Convergence studies	23
7	Demonstration of application of peridynamic modal analysis	25
8	Conclusions	27

1 INTRODUCTION

1.1 Novelty and Motivation

Commonly, structural damage is caused by design faults, construction quality shortcomings, or external effects such as improper use, overloading, natural disasters, environmental factors, etc. If such damage is not discovered and is allowed to grow, structure's load-bearing capacity deteriorates, which can lead to costly repairs or in extreme cases its collapse. Moreover, damage accumulates as a part of a structure's natural aging process. In situations as, for example, in Latvia where 37 % of all bridges are reported as either in poor or very poor condition, or in Europe where 35 % of its roughly half a million rail bridges are over 100 years old, accurate damage detection techniques can extend life of these structures and provide measurable economic benefit.

Modal analysis is widely used to detect structural damage, to control quality in manufacturing, to validate numerical models, etc. Modal properties – modal frequencies and mode shapes – depend on the object's mechanical and geometrical properties. When damage, such as cracks, is introduced in a structure, its geometrical and/or mechanical properties change. In principle, engineers should be able to detect the introduced damage from these changes. In practice, damage detection by modal analysis is difficult due to different limitations.

Additionally, there is a clear need for new and open computational modeling and simulation software that has been noted by the European Materials Modeling Council. Moreover, the need for new modeling software, particularly for engineering applications such as uncertainty quantification, risk analysis and decision in engineering, is recognized by the Council of the European Union in its decision that established the Horizon 2020 (H2020) framework programme for research and innovation.

Peridynamic theory or peridynamics (PD) is a non-local reformulation of classical continuum mechanics theory. Contrary to classical mechanics theory, the peridynamic theory represents forces and displacements using integral equations, which are defined even with discontinuous displacement fields. Damage in PD is introduced by breaking a bond according to some specified damage law, thus allowing for “spontaneous” crack formation. Meaning that they were not present initially, but formed after some damage criterion was exceeded. It follows that the crack path doesn't have to be specified *a priori*. Therefore, discontinuities are a natural part of a PD solution rather than a burden, thus making this theory an attractive option for damage modeling.

The author's preliminary studies showed that solving PD modal problems poses significant challenges. First, peridynamic stiffness matrices are non-symmetric, thus requiring non-Hermitian solvers and working with complex numbers. Secondly, PD stiffness matrices contain more non-zeros and their bandwidth is wider than finite-element (FE) equivalent. Thirdly, PD models usually consist of a large in number of nodes, which means that the matrix size is also large. These factors increase the computational cost of PD modal problems and can lead to poor solver convergence. Moreover, these simulations are frequently run on computing clusters, which require a massively parallel computational implementation. Therefore, a

considerable part of the research for this Thesis was devoted to finding and implementing a combination of solvers that solve PD modal problems in an efficient manner.

The scientific novelty of the presented research is the following.

- The well-known modal analysis has been implemented and studied in a new mechanic's theory – peridynamics – in which it has not been explored in detail before. The difference from the previous authors' work is that 3D rather than 2D problems are considered, which means that more than just bending modes are present. The results are verified and validated at several crack configurations rather than only at undamaged and a single damaged configuration, thereby providing more detailed analysis.
- This Thesis developed, implemented and optimized the first massively parallel and open-source PD modal solver in the world. Since it is open-source, it will be freely available to researchers in academia and industry, ensuring the sustainability of the research.

1.2 Aim and Scope

This Thesis aims to develop a novel massively parallel open-source modal solver for peridynamic modal problems, verify its results against finite-element modal analysis results, validate them against experimental modal analysis results, and demonstrate how PD modal analysis can be used together with PD damage simulations to obtain modal parameters of damaged structures.

This Thesis will not try to show that PD modal analysis is better than FE modal analysis and should be used in its place from now on. Rather the goal is to show that PD analysis is a viable alternative when considering problems where damage is present.

1.3 Tasks of the Thesis

To achieve the aim of the Thesis, the following tasks were set.

1. Develop and optimize a modal solver that can be efficiently run in a massively-parallel computing environment on a computing cluster and can solve a peridynamic modal problem.
2. Choose a test specimen and obtain its modal frequencies and mode shapes at nine different crack configurations using PD, FE, and experimental modal analysis. Then to verify and validate the PD results against the FE and the experimental results.
3. Consider several mesh densities and horizon lengths in the PD simulations to study the mesh convergence.
4. Demonstrate the use of PD modal analysis coupled with a fatigue damage simulation.

1.4 Practical Value of the Thesis

The developed computer code will be made freely accessible (open-source) to researchers and engineers worldwide. Thereby, ensuring that the results of this research can be practically applied and used in further research, rather than left lying on a shelf. Additionally, this will ensure the sustainability of the research.

Peridynamic theory represents forces and displacements using integral equations, which are defined even with discontinuous displacement fields, thus making damage modeling easier than in the continuum mechanics theory. By combining damage modeling and modal analysis the currently used techniques in numerical model validation, product design, manufacturing quality assurance, and structural damage detection are improved.

1.5 Arguments for the Defense of the Thesis

- The proposed peridynamic modal solver implementation has been optimized for use in a massively-parallel computational environment and can solve PD modal problems.
- The PD modal frequencies are in excellent agreement with the FE and the experimental modal frequencies in both undamaged and damaged configurations.
- The PD mode shapes agree well with and are in the same order as the FE mode shapes at a single crack configuration. The PD mode shapes also agree well with the experimental mode shapes. Moreover, the change in mode shapes from the introduced damage is similar in both analyses.
- The PD modal analysis can be coupled with PD damage simulations to simulate damage and obtain modal properties of the damaged object.

1.6 List of Attended Conferences

- 6th European Conference on Computational Mechanics, 7th European Conference on Computational Fluid Dynamics ECCM-ECFD 2018, Glasgow, UK, 11-15 June 2018. <http://www.eccm-ecfd2018.org/frontal/default.asp>
- 2018 International Symposium of Rail Infrastructure Systems Engineering (i-RISE 2018), Brno, Chechia
- International Modal Analysis Conference IMAC-XXXVI 2018, Orlando, Florida, USA, 12-15 February 2018 <https://semimac.org/event/imac-xxxvi/>
- The 3rd International Conference on Innovative Materials, Structures and Technologies IMST 2017, Riga, Latvia, 27-29 September 2017. <https://imst.rtu.lv/node/46>
- Modern building materials, structures, and techniques MBMST 2016, Vilnius, Lithuania, 26-27 May 2016. <http://mbmst.vgtu.lt/>

1.7 List of Publications

The following publications were published during the research for this Thesis. They are arranged in chronological order starting with the most recently published papers. Papers marked with an asterisk (*) are indexed either in SCOPUS or Web of Science databases.

1. Freimanis, A., Paeglītis, A. Modal Analysis of Healthy and Cracked Isotropic Plates in Peridynamics. *Conf. Proc. Soc. Exp. Mech. Ser.* 2019, 359–361, doi: 10.1007/978-3-319-74700-2_41. *
2. A. Freimanis, S. Kaewunruen, and M. Ishida, “Peridynamic Modeling of Rail Squats,” in *Sustainable Solutions for Railways and Transportation Engineering: Proceedings of the 2nd GeoMEast International Congress and Exhibition on Sustainable Civil Infrastructures*, 2019, pp. 108–118.
3. Freimanis, A., Kaewunruen, S. Peridynamic Analysis of Rail Squats. *Appl. Sci.* 2018, 8, 2299, doi: 10.3390/app8112299. *
4. Kaewunruen, S., Janeliukstis, R., Freimanis, A., Goto, K. Normalised curvature square ratio for detection of ballast voids and pockets under rail track sleepers. *J. Phys. Conf. Ser.* 2018, 1106, 012002, doi: 10.1088/1742-6596/1106/1/012002. *
5. S. Kaewunruen, A. Freimanis, and M. Ishida, “EFFECT OF EXTREME CLIMATE ON WHEEL-RAIL INTERACTION OVER RAIL SQUATS,” in *Proceedings of the 6th. European Conference on Computational Mechanics (Solids, Structures and Coupled Problems) ECCM 6, 7th. European Conference on Computational Fluid Dynamics ECFD 7*, 2018, pp. 11–15.
6. Freimanis, A., Kaewunruen, S., Ishida, M. Peridynamics Modelling of Rail Surface Defects in Urban Railway and Metro Systems. *Proceedings 2018*, 2, 1147, doi: 10.3390/proceedings2161147.
7. Freimanis, A., Paeglītis, A. Mesh Sensitivity in Peridynamic Quasi-static Simulations. *Procedia Eng.* 2017, 172, 284–291, doi: 10.1016/j.proeng.2017.02.116. *
8. Freimanis, A.; Paeglītis, A. Modal analysis of isotropic beams in peridynamics. *IOP Conf. Ser. Mater. Sci. Eng.* 2017, 251, 012088, doi: 10.1088/1757-899X/251/1/012088.*
9. Paeglītis, A., Freimanis, A. Comparison of constant-span and influence line methods for long-span bridge load calculations. *Balt. J. Road Bridg. Eng.* 2016, 11, 84–91, doi:10.3846/bjrbe.2016.10. *
10. Freimanis, A., Paeglītis, A. Analysis of Yearly Traffic Fluctuation on Latvian Highways. *IOP Conf. Ser. Mater. Sci. Eng.* 2015, 96, 012064, doi: 10.1088/1757-899X/96/1/012064. *

2 THEORY BACKGROUND

2.1 Peridynamic Theory

A peridynamic body consists of a number of nodes each uniquely described by its volume V_i , density ρ_i and position vector in the reference configuration \mathbf{x}_i . An example of 2D body is shown in Figure 2.1. Node \mathbf{x}_i interacts with other nodes \mathbf{x}_j through bonds (relative position vectors) $\boldsymbol{\xi}_{ij} = \mathbf{x}_j - \mathbf{x}_i$. These interactions are limited to a range called the horizon δ . Nodes \mathbf{x}_j that are connected to \mathbf{x}_i are called the family of \mathbf{x}_i , \mathbf{H}_{x_i} .

When a body deforms, node \mathbf{x}_i experiences displacement \mathbf{u}_i and moves to its deformed position $\mathbf{y}_i = \mathbf{x}_i + \mathbf{u}_i$. The bond in the deformed configuration is $\mathbf{y}_j - \mathbf{y}_i$. This deformation creates a bond force density vector \mathbf{t}_{ij} that depends on the collective deformation of all nodes in \mathbf{H}_{x_i} and an opposite bond force density vector \mathbf{t}_{ji} that depends on the collective deformation of \mathbf{H}_{x_j} . Bond forces are force densities (force per volume), not stresses (force per area), because each node describes some volume. The bond deformation vectors are stored in an array called the deformation state

$$\mathbf{Y}_{x_i} = \begin{Bmatrix} \mathbf{y}_1 - \mathbf{y}_i \\ \vdots \\ \mathbf{y}_n - \mathbf{y}_i \end{Bmatrix}, \quad (2.1)$$

similarly, the force density vectors are stored in an array called the force state

$$\mathbf{T}_{x_i} = \begin{Bmatrix} \mathbf{t}_{i1} \\ \vdots \\ \mathbf{t}_{in} \end{Bmatrix}. \quad (2.2)$$

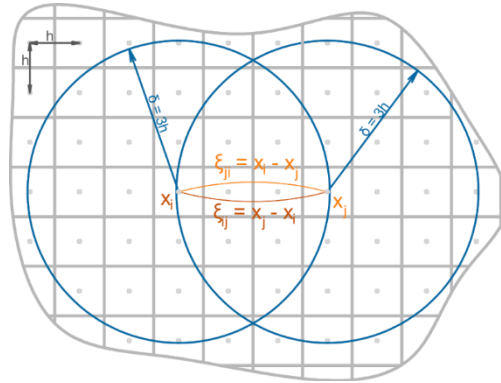


Fig. 2.1. A discretized two-dimensional PD body B . Only two bonds – $\boldsymbol{\xi}_{ij}$ and $\boldsymbol{\xi}_{ji}$ – are showed. Both are showed curved to avoid overlapping.

The bond force density vectors are computed using bond deformations:

$$\mathbf{T}(\mathbf{x}_i) = \mathbf{T}(\mathbf{Y}(\mathbf{x}_i)), \quad (2.3)$$

where function $\mathbf{T}(\mathbf{x}_i)$ is a material model. It is common to write $\mathbf{T}(\mathbf{x}_i)\langle\mathbf{x}_j - \mathbf{x}_i\rangle$, or $\mathbf{T}(\mathbf{x}_i)\langle\xi_{ij}\rangle$ when referring to force density vector \mathbf{t}_{ij} in a bond $\xi_{ij} = \mathbf{x}_j - \mathbf{x}_i$, and similarly for deformation state and deformed bond vectors. The peridynamic equation of motion in the integral form is

$$\rho(\mathbf{x}_i)\ddot{\mathbf{u}}(\mathbf{x}_i, t) = \int_{H_{\mathbf{x}_i}} (\mathbf{T}(\mathbf{x}_i)\langle\mathbf{x}_j - \mathbf{x}_i\rangle - \mathbf{T}(\mathbf{x}_j)\langle\mathbf{x}_i - \mathbf{x}_j\rangle) dV_{\mathbf{x}_j} + \mathbf{b}(\mathbf{x}_i), \quad (2.4)$$

where $\rho(\mathbf{x}_i)$ – density,

$\ddot{\mathbf{u}}(\mathbf{x}_i, t)$ – acceleration,

$\mathbf{b}(\mathbf{x}_i)$ – external force density.

Contribution of a bond to the force density at a node can be weighed using influence function $\omega(\mathbf{x}_i)$. The value of an influence function can depend on the length, direction or other bond properties. It can also be used to introduce damage; remove interaction between two nodes by setting the influence function to 0 i.e. break the bond, when some damage criterion is reached. The simplest damage criterion could be the critical stretch in which a bond breaks when it is stretched past some critical value s_c :

$$\omega(\mathbf{x}_i) = \begin{cases} 1, & \text{if } s_{ij} < s_c, \\ 0, & \text{if } s_{ij} \geq s_c, \end{cases} \quad s_{ij} = \frac{|\mathbf{y}_j - \mathbf{y}_i| - |\mathbf{x}_j - \mathbf{x}_i|}{|\mathbf{x}_j - \mathbf{x}_i|} = \frac{|\mathbf{Y}\langle\xi_{ij}\rangle| - |\xi_{ij}|}{|\xi_{ij}|}, \quad (2.5)$$

where s_{ij} – bond stretch. Then the damage at a node can be defined as a ratio between the broken and the initial number of bonds:

$$\phi(\mathbf{x}_i) = 1 - \frac{\int_{H_{\mathbf{x}_i}} \omega(\mathbf{x}_i) dV_{\mathbf{x}_j}}{\int_{H_{\mathbf{x}_i}} dV_{\mathbf{x}_j}}. \quad (2.6)$$

2.2 Linear Algebra and Modal Analysis

When damping of a system is small, it is commonly ignored and the equation of motion takes the following form:

$$\mathbf{M}\ddot{\mathbf{u}} + \mathbf{K}\mathbf{u} = \mathbf{F}, \quad (2.7)$$

where the mass matrix \mathbf{M} describes the mass of each node in a body and the stiffness matrix \mathbf{K} describes the stiffness that node \mathbf{x}_i exerts on node \mathbf{x}_j and vice versa.

Free vibrations of a multiple DOF system are initiated by the presence of an initial potential or kinetic energy so $\mathbf{F} = 0$. Equation (2.7) can be rewritten as

$$\mathbf{K}\mathbf{x} = \lambda\mathbf{M}\mathbf{x}. \quad (2.8)$$

In linear algebra Equation (2.8) is called a generalized eigenvalue problem. Values λ and \mathbf{x} that satisfy this equality are called eigenvalues and eigenvectors respectively. Eigenvectors \mathbf{x} are also mode shapes. Eigenvalues λ are related to modal frequencies f through (2.13).

Methods for solving equations are either direct or iterative and the computer algorithms that solve these equations are called solvers. Direct methods will reach an exact solution, if it exists, in some finite number of steps. Whereas iterative methods obtain an approximation of \mathbf{x} that is often good enough for practical applications. Iterative methods start from some initial guess \mathbf{x}_0 and in each step produce a new guess \mathbf{x}_{n+1} that is slightly closer to the exact solution. When the difference between \mathbf{x}_n and \mathbf{x}_{n+1} (the residual) falls below some specified tolerance value, the computation is stopped and it is said that the result has converged. Generally, iterative methods use less memory because the whole matrix does not need to be stored.

Preconditioning is a technique used in iterative solvers that modify the original problem making it easier to solve. The best known is the so-called shift-invert technique. A generalized eigenvalue problem in (2.8) is transformed into

$$\mathbf{C}\mathbf{x} = \theta\mathbf{x}, \quad (2.9)$$

where both \mathbf{C} and θ are substitutions

$$\mathbf{C} = (\mathbf{A} - \sigma\mathbf{B})^{-1}\mathbf{B} \quad (2.10)$$

and

$$\theta = (\lambda - \sigma^2)^{-1}, \quad (2.11)$$

where σ – shift value. Now (2.9) is a simple eigenvalue problem. When a shift σ is chosen well, eigenvalues of matrix \mathbf{C} are better separated than those of \mathbf{K} , which leads to faster convergence. If a solver converged, then obtained eigenvectors \mathbf{x} are the same as eigenvectors for the original problem, but eigenvalues need to be reinverted and shifted back:

$$\lambda = \frac{1}{\theta} + \sigma^2. \quad (2.12)$$

Then obtained eigenvectors \mathbf{x} are the mode shapes of the original problem in (2.8), but modal frequencies f are calculated from eigenvalues that have to be reinverted and shifted back:

$$f = \frac{+\sqrt{\frac{1}{\theta} + \sigma^2}}{2\pi}. \quad (2.13)$$

3 COMPUTATIONAL IMPLEMENTATION AND OPTIMIZATION

PD simulations were run on computing cluster *Vasara* at Riga Technical University. Different numbers of Dell EMC PowerEdge R640 nodes, each with $2 \times$ Intel(R) Xeon(R) Gold 6154 3.00 GHz CPUs with 36 cores, were used. Each node had 348 GB maximum available RAM and a 240 GB SSD. They were connected through Infiniband EDR 100 Gb/s connection. The cluster ran Centos 7.5 operating system and used Torque 6.1.1.1 resource manager. The modal solver was implemented by extending Peridigm 1.5.0, which at the time of writing was available at <https://github.com/peridigm/peridigm>.

3.1 Peridynamic Implementation

Modal Solver

During the research for and the development of this Thesis it became clear that solving PD modal problems poses significant challenges.

- First, peridynamic stiffness matrices are non-symmetric, thus require non-Hermitian solvers. Generally, non-symmetric matrices take up more computer memory, because the whole matrix rather than only half needs to be stored. Furthermore, the eigenvalues of non-symmetric problems need not be real, so solutions involve working with complex numbers.
- Secondly, a node in PD is generally connected to more nodes than a node in FE analyses, so the stiffness matrices contain more non-zeros and their bandwidth is wider. As the number of non-zero elements increases, the required memory also increases. Moreover, more non-zeros lead to poorer convergence, because there are more values to consider.
- Thirdly, for practical problems, PD models consist of a large number of nodes, possibly in the millions. In small models (with large node spacings), the crack tip would advance in large jumps, which poorly describe the behavior of a crack. Reasonable mesh convergence can be achieved only with large models and, if node spacings are large, the boundary conditions can have a disproportionate effect on the behavior of the model, thus Saint-Venant's principle will not be met.

The modal solver was implemented in open-source peridynamics code Peridigm. Since it is an open-source software, the author could later contribute the written code making this analysis available to other researchers and engineers. Moreover, several Peridigm's parts – material models, stiffness matrix creation routines, discretization – could be reused, thus reducing the time spent on writing the code for a working modal solver.

A combination of ILU preconditioner, flexible block-GMRES linear solver, and block Krylov-Schur eigensolver were implemented. The Trilinos library was used to implement the solver due to the following:

- Peridigm is already built using several packages from Trilinos, so further integration was easier;

- Trilinos is designed for massively parallel computations making it well suited for running on a computing cluster;
- All three – linear solvers, eigensolvers and preconditioners – are available in Trilinos, therefore only one library needs to be used for implementation.

Peridynamic Model

A simple rectangular plate was used. Common real-life structures would have a more complex shape, but a simple shape is sufficient to verify and validate results. Also, it was a good choice, because different types of modes were present.

Peridigm uses a meshfree discretization. Its mesh files, which are text files with each line describing a single node, must be supplied by the user. Required data are node's x , y , z coordinate, block ID, and volume. A block is a group of nodes to which a material model, damage model, and contact model are prescribed. Four models with 40 000, 135 000, 320 000, and 625 000 nodes were used. The nodal spacing h was the same in all three directions: 0.001 m, 0.000667 m, 0.0005 m and 0.0004 m respectively. The model size was 0.10 m \times 0.05 m \times 0.008 m. In this Thesis the horizon values $\sqrt{2}h, 2h, 3h, 4h$ are used.

Simulations used Linear Peridynamic Solid material model, which is the PD equivalent of an elastic material model in the continuum mechanics. To create free-free test conditions, no boundary conditions were applied. The material properties were: elastic modulus – 5.35 GPa; Poisson's ratio – 0.33; density – 1200 kg/m³.

Cracks in a model were created by specifying a crack plane and breaking any bond that crosses this plane. Crack configurations and locations are presented in Chapter 4.

The first 12 modes were computed. The first six were the rigid-body-motion modes, so only the next six were compared with the FE and the experimental results.

3.2 Finite-Element Implementation

Modal analysis in the finite-element method is well understood and widely used in both research and engineering, therefore, it was a natural choice for verification of PD results. A rectangular plate model with the same measurements as the PD model was created using Ansys FE software. An elastic material model was used, and the material properties were the same as for the PD simulations. The FE model was meshed using SOLID185 8-node cubic elements and contained 664 146 nodes.

This kind of problem could have been modeled using shell elements, which would have been computationally less expensive, however, solid elements were chosen for two reasons:

- the author wanted FE and PD meshes to have a similar number of nodes;
- it was possible to create cracks through the depth of the FE model, which would not have been possible if the model was created using shell elements; cracks in the FE model were created by not connecting the nodes of solid elements on a crack plane.

3.3 Solver Parameter Optimization

Solver parameters influence the solve time, memory use, and whether a simulation will converge at all. Mathematical optimization is the selection of the best element with regards to some criterion from some set of available alternatives. In this Thesis, maximum memory use and computation time are the two objectives that were optimized. The maximum memory used was gathered from “tracejob” command that is available in the Torque resource management system, but the length of a simulation was measured by Peridigm’s built-in timer.

Commonly, Pareto optimization is used for multi-objective optimization problems. For the present case, a Pareto optimal would be such a solver parameter combination that it is impossible to change any single solver parameter without making either the memory use higher or the solve speed slower. Usually, a set – called a Pareto frontier – of such Pareto optimal points can be found.

Table 3.1

Test Cases and Their Parameters

Case	NEV	Horizon	Number of experiments	Converged	Did not converge	Exceeded memory
A	1	$\sqrt{2}h$	180	131	15	34
B	10	$\sqrt{2}h$	150	105	7	38
C	1	$3h$	150	142	0	8
D	10	$3h$	150	124	0	26

Model dimensions, material model, material properties and boundary conditions are the same as described previously. The model was discretized with 135 000 nodes and the nodal spacing was $h = 0.000667$ m.

Test values were selected using Latin-Hypercube sampling technique. Four cases – named A through D – were considered. They differed by the number of eigenvalues (NEV) – 1 or 10 – and the length of the horizon – either $\delta = \sqrt{2}h$ or $\delta = 3h$. Specific values are showed in Table 3.1. The solver tolerances were set to $1e^{-6}$ and $1e^{-4}$ for linear solver and eigensolver respectively.

Table 3.2

Solver Parameters Used for Peridynamic Modal Analysis

Parameter	Value
ILU level of fill	1
ILU Drop tolerance	$1e^{-6}$
ILU Overlap level	0
Linear Solver Max Restarts	10
Linear Solver Number of Blocks	1000
Linear Solver Block Size	6
Eigensolver Max Restarts	10
Eigensolver Number of Blocks	12
Eigensolver Block Size	3

The total number of simulations, converged and unconverged, and the number of simulations that exceeded available memory are shown in Table 3.1. Case A has more tests than the rest because a larger part of them exceeded available memory and was, therefore, killed by the operating system. 73 %, 70 %, 95 % and 83 % of all simulations converged for cases A through D respectively.

Several relations between the solver parameters, simulation time and memory use were found. They are discussed in detail in the full Thesis. Table 3.2 shows parameter values that were used for modal simulations in the Thesis.

4 SPECIMEN MANUFACTURING AND EXPERIMENTAL SETUP

Two kinds of specimens were used: dog-bone tensile specimens to obtain mechanical properties, and rectangular plates to obtain modal properties. All specimens were cut from 8 mm polymethyl methacrylate (PMMA) sheets using laser cutting. PMMA was chosen, because it is isotropic, easy to obtain, cheap, easy to cut into shape, easy to work with (not as heavy as concrete, smelly as asphalt, abrasive as glass fiber).

Tensile tests were done according to ASTM D638 standard. Nine specimens were tested and the average values were used as inputs in simulations. The mechanical properties are presented in Chapter 3.

Ten $0.1 \text{ m} \times 0.05 \text{ m} \times 0.008 \text{ m}$ large plate specimens were used for modal testing. Their average density was 1187.34 kg/m^3 . Nine different crack configurations and two crack types were considered, see Figures 4.1. Five specimens were tested at each crack configuration. Configurations were named by crack type and a letter in alphabetical order, e.g. Sd. Letter “a” was reserved for the Healthy configuration.

- Undamaged specimens were called Healthy configuration.
- Specimens with a crack through their thickness were called T crack configuration.
- Specimens with a crack on their back face were called S crack configuration.

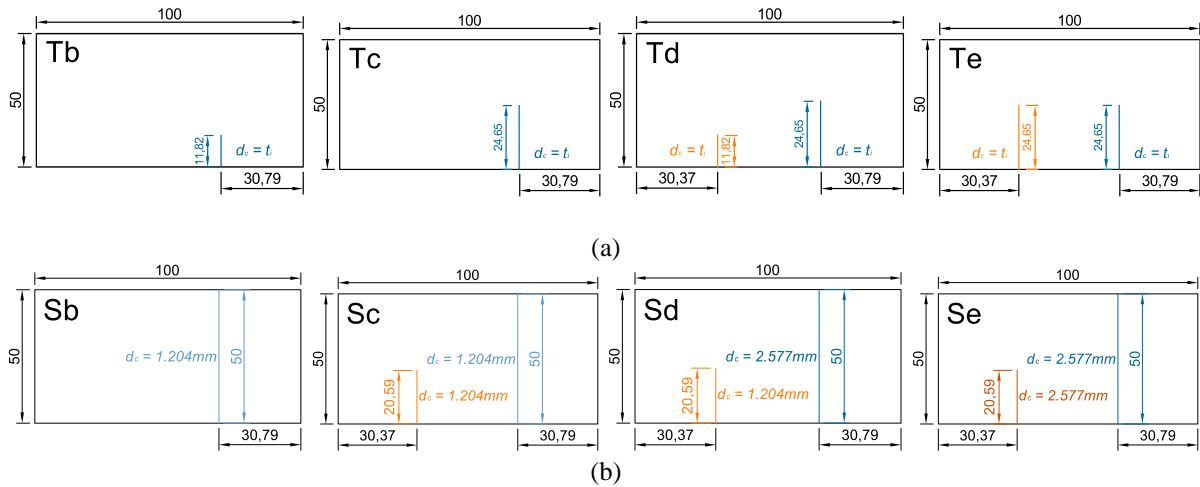


Fig. 4.1. Crack location, length, and depth. d_c – depth of a crack; t_i – the thickness of a plate; a – T crack configuration; b – S crack configuration.

Four approaches to crack creation were considered – laser cutting, using a jeweler’s saw, using a sharp razor blade, growing a fatigue crack. The method had to be fast, precise, and it had to be possible to extend a crack later. Jeweler’s saw, razorblade and fatigue crack growth created roughly but not the same crack path in all specimens. Furthermore, the crack length when a crack was extended was not sufficiently similar across all five specimens. So only laser cutting fit all three criteria.

Modal test specimens were suspended from an aluminum frame in two loops made from cotton thread to allow specimens to move as free as possible, thus creating free-free boundary conditions (BC). Measurements were done using 2D Polytec PSV-400 laser vibrometer. Paper tape was applied on the specimen surface, to prevent the laser beam from shining through. Specimens were excited using a loudspeaker. Measurement range was between 1000 Hz and 8000 Hz with measurement step $\Delta f = 2.5$ Hz.

5 VERIFICATION AND VALIDATION OF PERIDYNAMIC MODAL ANALYSIS

Results were grouped by their crack configurations – Healthy, Tb through Te, and Sb through Se. The mode order changed between different crack configurations, so it was not possible to refer to individual modes by their number in the order of appearance, hence, modes will be referred to by their type and number within that type, e.g. 2nd bending mode, 1st torsional mode, etc. PD modal analysis was used to compute 864 modes, FE analysis – 54 modes, and 240 modes were measured using experimental modal analysis. For exact modal frequency values please see the full Thesis.

Only the 1st and the 2nd bending and the 1st and the 2nd torsional modes were computed with PD and FE analysis at all T and S crack configurations. Additionally, the 1st transversal bending mode was computed at all S configurations. Only these modes will be used for verification and validation. Other modes were computed only at some configurations, because the mode order changed. Only results computed with the shortest horizon $\delta = \sqrt{2}h$ and the longest horizon $\delta = 4h$ will be used here. They show a comparison between the most local and the most non-local result while keeping figures easy to read.

Three different computer programs – Paraview, Ansys, and Polytec Scan Viewer – were used to visualize the PD, FE and experimental mode shapes respectively. The programs used similar, but not completely identical, color schemes. The color distribution in the mode shapes, therefore, can appear slightly different.

Verification and Validation of the PD Modal Frequencies

The percentage difference between the PD and the FE modal frequencies at Healthy and T crack configurations are presented in Figure 5.1. Please see the full Thesis for S configuration plots. Differences between the PD and the FE results were expected because the same problem was solved by two different mechanics theories, but the results show a very good agreement. The largest difference between modal frequencies when $\delta = \sqrt{2}h$ is 2.37 % at Te crack configuration for the 2nd torsional mode. When $\delta = 4h$ the largest difference is –3.92 % at Te crack configuration for the 2nd torsional mode. For S crack configurations, the results show an excellent agreement between the PD and the FE modal analyses. The percentage difference between PD and FE results ranged from –2.02 % to +1.47 %.

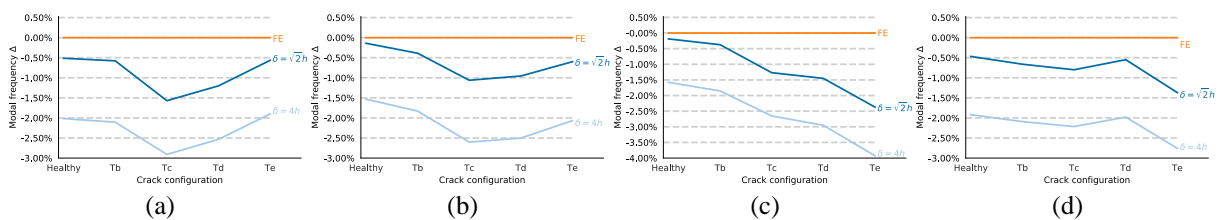


Fig. 5.1. The percentage difference between PD modal frequencies and FE modal frequencies at T crack configurations. a – 1st bending mode; b – 1st torsional mode; c – 2nd torsional mode; d – 2nd bending mode.

PD modal frequencies were lower than FE modal frequencies at Healthy and all T crack configurations. The differences in computed modal frequencies most likely occurred due to different stiffness matrices. The PD computational stiffness must have been lower than the FE computational stiffness. PD results with the horizon $\delta = \sqrt{2}h$ agreed better with the FE results than simulations with the horizon $\delta = 4h$ at most crack configurations. This was expected, because the non-local PD solution approaches the local solution when the horizon shrinks to zero.

The percentage difference between PD, experimental and FE modal frequencies at Healthy and T crack configurations are presented in Figure 5.2. S crack configuration results are presented in the full Thesis. PD modal analysis is at least just as accurate as FE modal analysis for the used test conditions. Additionally, the differences between the PD results and the experimental results are very low, which shows that PD modal analysis closely reflects the modal behavior of the test specimens. At T crack configurations, the difference between PD and experimental results were within -3.20% to 2.59% , but between FE and experimental results within -1.20% to 3.57% . At S crack configurations, the difference between the PD and the experimental results ranged between -1.81% and 3.06% , but between FE and experimental results between -1.26% and 2.96% .

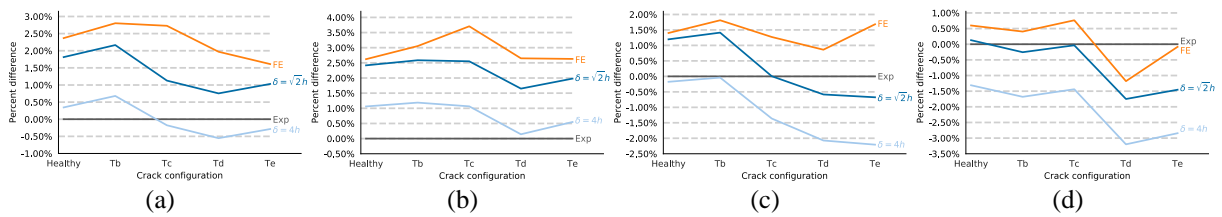


Fig. 5.2. The percentage difference between PD, experimental, and FE modal frequencies at T crack configurations. a – 1st bending mode; b – 1st torsional mode; c – 2nd torsional mode; d – 2nd bending mode.

Frequency Shift

The frequency shift is the change in modal frequencies when an object’s stiffness changes due to the introduction of damage or other influences. Modal frequencies vary between 1000 Hz and 7000 Hz, so relative frequency shifts will be presented.

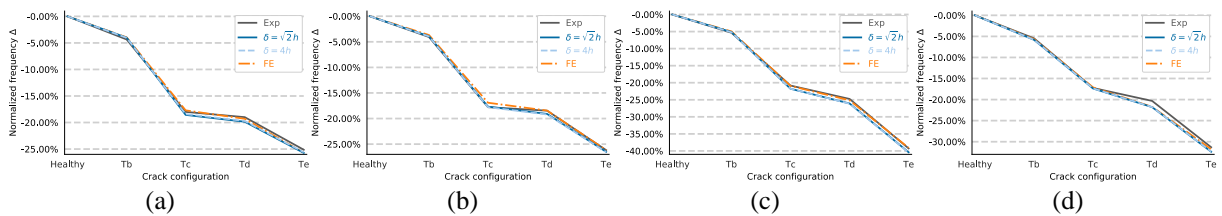


Fig. 5.3. Relative frequency shift in T crack configuration specimens. a – 1st bending mode; b – 1st torsional mode; c – 2nd torsional mode; d – 2nd bending mode.

See Figure 5.3 for T configuration shifts, but for S configuration plots see the full Thesis. At Te crack configuration the largest shift is -40.46% , but the smallest shift -25.61% , but at Se configuration the largest shift is -7.82% , but the smallest was -0.24% . The results show

14.85 and 7.58 percentage point difference between the largest and the smallest shift at Te and Se configuration respectively. This means that crack influence on the stiffness of PD models differs considerably depending on the mode considered.

The agreement between the PD, the FE, and the experimental frequency shift was excellent. At Te crack configuration the differences between PD and FE frequency shifts ranged between -1.38 and -0.04 percentage points, but between the PD and the experimental relative frequency shifts between -1.47 and $+0.34$ percentage points. At Se crack configuration, the difference in PD and FE shifts ranged between -0.19 and 1.30 percentage points, but between the PD and the experimental shifts between -0.70 and $+1.95$ percentage points.

Verification of PD Mode Shapes

Mode shapes for Te, and Se crack configurations will be presented in Figures 5.5 and 5.6 respectively. Other modes are presented in the full Thesis. A color legend with numerical values cannot be provided, because a mode shape is a dimensionless representation of a structure vibrating at a modal frequency. The whole color scheme is shown in Figure 5.4.



Fig. 5.4. The color scheme used in figures 5.5 and 5.6.

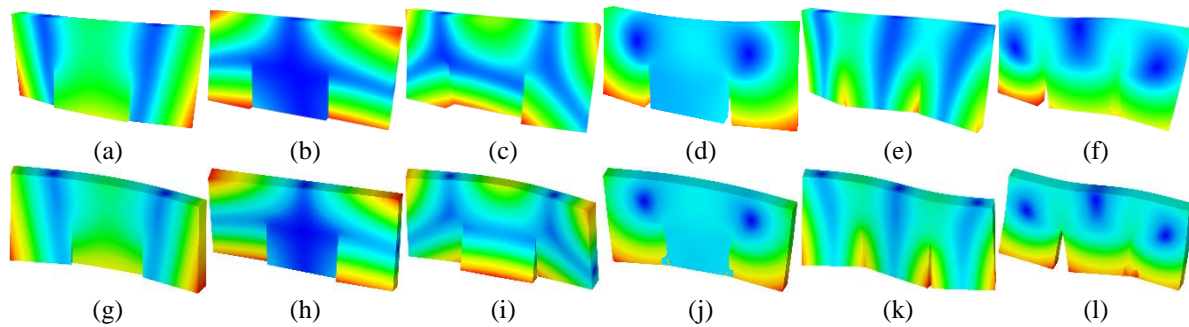


Fig. 5.5. PD and FE mode shapes at Te configuration. Top – PD mode shapes, bottom – FE mode shapes. a, g – 1st bending mode; b, h – 1st torsional mode; c, i – 2nd torsional mode; d, j – 1st in-plane bending mode; e, k – 2nd bending mode; f, l – 2nd in-plane bending mode.

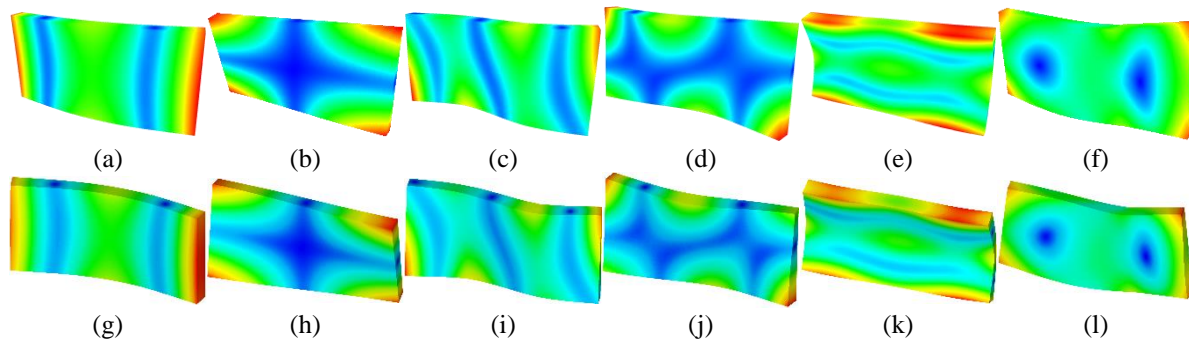


Fig. 5.6. PD and FE mode shapes at Se configuration. Top – PD mode shapes, bottom – FE mode shapes. a, g – 1st bending mode; b, h – 1st torsional mode; c, i – 2nd bending mode; d, j – 2nd torsional mode; e, k – 1st transversal bending mode; f, l – 1st in-plane bending mode.

PD modal analysis and FE modal analysis yielded the same mode shapes at every single crack configuration. At Te crack configuration, Figure 5.5, the mode order was: the 1st bending, the 1st torsional, the 2nd torsional, the 1st in-plane bending, the 2nd bending, the 2nd in-plane bending mode. At Se crack configuration, Figure 5.6, the mode order was: the 1st bending mode, the 1st torsional mode, the 2nd bending mode, the 2nd torsional mode, the 1st transversal bending mode, the 1st in-plane bending mode.

The introduced cracks created a sudden discontinuity in the displacement field and the displacement field shifted in response. This can be seen in both T and S crack configuration mode shapes. For example, for the 1st torsional mode at Te configuration – Figures 5.5b and 5.5h – maximum displacements are located at the two top corners and also at the whole bottom side to the left from the left crack and to the right from the right crack. At Se configurations, there are no visible changes for the 1st bending, torsional, transversal bending, and in-plane bending modes shapes. For the 2nd torsional mode, the zero displacement area to the left has visibly shifted downwards. But for the 2nd bending mode the three blue zero displacement areas are no longer parallel to the short edges. Cracks were visible in all PD and FE mode shapes at T crack configurations, but not at S configurations, because the cracks were located on the back face of the model.

Validation of the PD Mode Shapes

The results for the 1st bending mode at both crack configurations will be presented in Figures 5.8 and 5.9. Please see the full Thesis for other mode shapes. Only 2D modes could be obtained from the experimental analysis due to limitations of the available equipment. The author chose to present also the PD modes in 2D so that they can be compared with the experimental data more easily. The color scheme used in this chapter is presented in Figure 5.7.



Fig. 5.7. The color scheme used in figures 5.8 and 5.9.

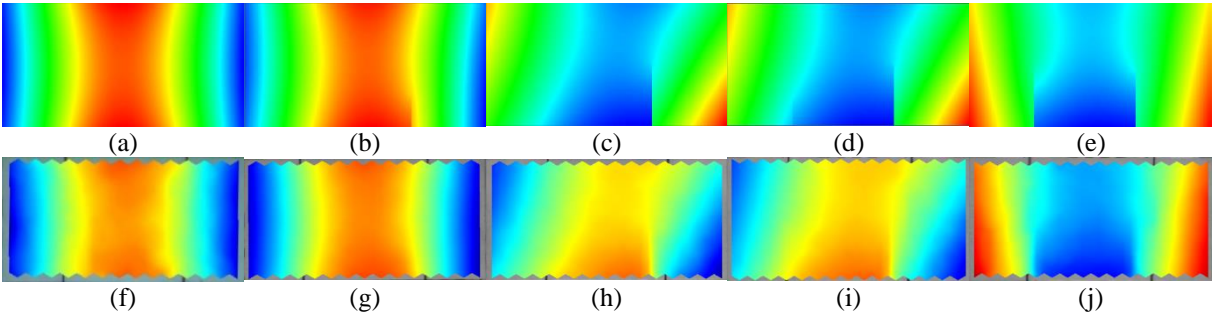


Fig. 5.8. Mode shapes of the 1st bending mode. Top row – PD, bottom row – experimental modes shapes. a, f – Healthy; b, g – Tb; c, h – Tc; d, i – Td; e, j – Te configuration

The PD and the experimental mode shapes are in excellent agreement. For T configuration, the extreme displacements are located in the middle and at both ends. When cracks are introduced, displacement shift in response and the introduced cracks are clearly visible in all PD mode shapes, but not in all experimental mode shapes. Cracks in S configurations were manufactured into the back face of a specimen, not through specimen thickness. Therefore, they did not appear on the specimen surface, also the 1st bending mode's displacement field did not visibly shift when cracks were introduced.

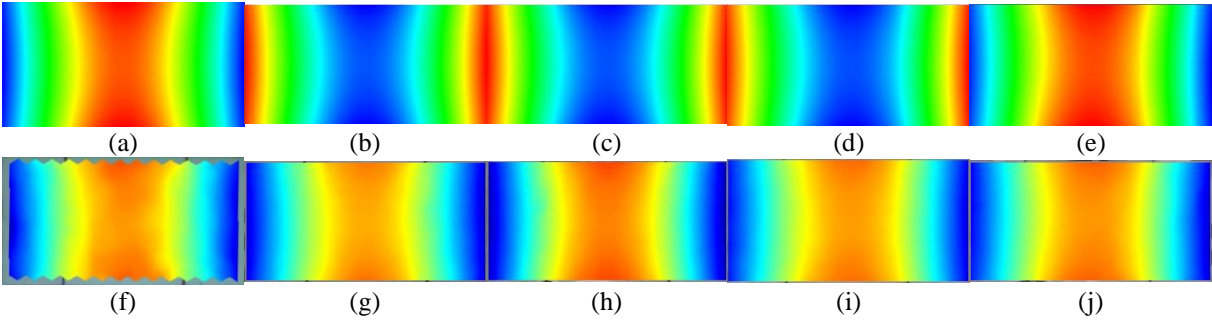


Fig. 5.9. Mode shapes of the 1st bending mode. Top – PD, bottom – experimental modes shapes. a, f – Healthy; b, g – Sb; c, h – Sc; d, i – Sd; e, j – Se configuration.

6 CONVERGENCE STUDIES

Every acceptable numerical method should converge or at least tend to the exact local or non-local solution, thus meshes with a higher number of nodes, i.e. a smaller node spacing, should produce more accurate results at an increased computational cost. Mesh or grid convergence is, therefore, studied to determine the lowest number of nodes in a model with an acceptable discretization error.

A model has some number of nodes m and the inverse property – mesh spacing – is h . Discretization error is an error that arises when a function of a continuous variable is represented by a finite number of evaluations. As the mesh spacing decreases, i.e. $h \rightarrow 0$, the discretization error should asymptotically approach zero and only computer round-off errors should remain.

In PD three types of convergence can be defined:

- The δm -convergence where $\delta \rightarrow 0$ and m increases as δ decreases, with m increasing faster than δ decreases. The numerical PD solution will converge to the analytical PD solution and converge to the local continuum mechanics solution.
- The m -convergence where δ is fixed and $m \rightarrow \infty$. In this case, the PD solution converges to the exact non-local PD solution for a given δ .
- The δ -convergence where $\delta \rightarrow 0$ and m is fixed or increases with decreasing δ . In this case, the PD solution converges to an approximation of the continuum mechanics solution.

It must be noted that in a computational model the horizon δ is required to cover more than its own node, so it cannot shrink to zero. In these Thesis the shortest horizon used is $\delta = \sqrt{2}h$.

Two convergence studies – δ and δm – were done. In the δ -convergence study, mesh density was held constant at either 40 000, 135 000, 320 000 or 625 000 nodes while the horizon shrank from $\delta = 4h$ to $\delta = \sqrt{2}h$. But in the δm -convergence study the horizon was held constant at either $\delta = \sqrt{2}h$, $\delta = 2h$, $\delta = 3h$ or $\delta = 4h$ while the mesh density increased from 40 000 to 625 000 nodes.

Convergence studies are presented for simulations at Healthy configuration δm -convergence plots and for the first six modes are presented in Figure 6.1. All presented plots show that the computed modal frequencies approach the continuum value asymptotically as the mesh density increases.

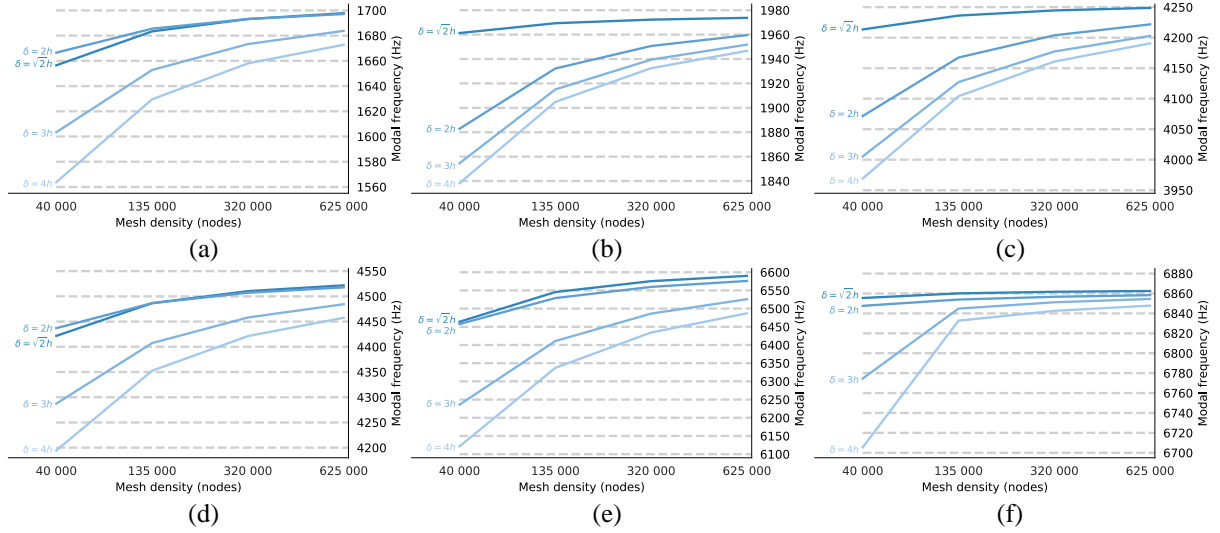


Fig. 6.1. δm -convergence at Healthy configuration. a – 1st bending mode; b – 1st torsional mode; c – 2nd torsional mode; d – 2nd bending mode; e – 1st transversal bending mode; f – 1st in-plane bending mode.

The computed δm -convergence orders showed that in all cases convergence is not linear but of some higher order $p > 1$, which means that even little increase in mesh density gives a large gain in accuracy. Generally, it is between 1 and 2 so it does not reach quadratic convergence.

δ -convergence plots are presented only in the full Thesis. It is noted that since mesh spacing does not shrink in δ -convergence, it need not be asymptotic. For the first two bending modes and the 1st transversal bending mode in values converged rapidly till $\delta = 2h$ and did not change significantly when horizon decreased to $\delta = \sqrt{2}h$. The 1st and the 2nd torsional mode's results tend to a single value at $\delta = \sqrt{2}h$ with no exceptions. Lastly, the results of the 1st in-plane bending mode converge in the same way as the results for other modes.

7 DEMONSTRATION OF APPLICATION OF PERIDYNAMIC MODAL ANALYSIS

Modal analysis was combined with the PD fatigue simulation. First, modal analysis was performed using an undamaged specimen, then fatigue simulation was run, followed by another modal analysis. The first 12 modes were computed and no boundary conditions were applied in both modal analyses. The first six were rigid-body motion modes that will not be used hereafter.

A dog-bone tensile test specimen was used for demonstration. Its dimensions are presented in Figure 7.1a. The horizon was set to 0.0015001 m and there were 204 000 nodes in the model. Simulations were run using an elastic material model. The material parameters were: density – 7850.0 kg/m³; Poisson’s ratio – 0.30; and Young’s modulus – 189.9 GPa. In the fatigue simulation, constant displacement of $9e^{-5}$ m was applied at both ends in the opposite y directions. Boundary conditions were applied to groups of nodes within one horizon from either end. Additionally, the damage was disabled for any node within 3δ from both ends to avoid any unphysical behavior close to the BCs. Parameters for the fatigue model are presented in Table 7.1. The fatigue simulation ran for 870 000 cycles and the model at the end of the simulation is shown in Figure 7.1b. Two cracks on the opposite sides of the narrowest part of the specimen grew towards each other and then each crack split into two.

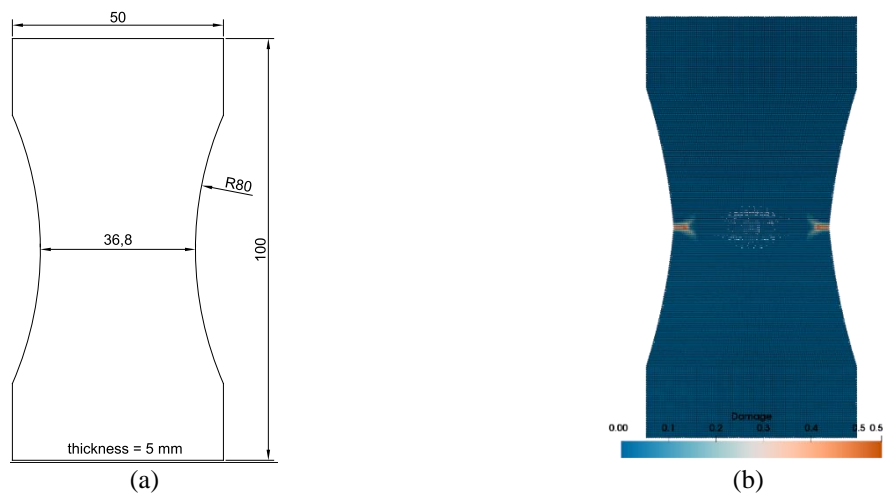


Fig. 7.1. The model used for demonstration. a – the model with its dimensions; b – damage after 870 000 fatigue cycles.

Table 7.1

Parameters of Fatigue Damage Model

Parameter	Value
A_I	426.00
m_I	2.77
A_{II}	25237.48
m_{II}	4.00
ϵ_∞	0.00186
Φ_C	0.385

Modal frequencies are presented in Table 7.2, color scheme for the mode shapes in Figure 7.2 and the first three mode shapes in figure 7.3, other shapes can be seen in the full Thesis. All modal frequencies experienced frequency shift when the fatigue cracks were introduced. The largest frequency shift was -2.91% for the 1st bending mode, and it was smaller for other modes in absolute and relative values. This shows that the peridynamic theory allows for realistic and naturally evolving damage simulations coupled together with modal analysis for damage assessment. Introduced fatigue damage has not visibly changed mode shapes. However, quantitative rather than qualitative assessment should be done to assess the difference between mode shapes before and after fatigue damage. Such a study is outside the scope of this Thesis.



Fig. 7.2. The color scheme used in Figure 7.3.

Table 7.2

Modal Frequencies of Undamaged Model and Damaged Model After 870 000 Cycles

Mode	Undamaged model (0 cycles)		Damaged model (870 000 cycles)		Δf %
	Mode type	f , Hz	Mode type	f , Hz	
1 st	1 st bending	2446.38	1 st bending	2377.17	-2.91%
2 nd	1 st torsional	2949.17	1 st torsional	2911.42	-1.30%
3 rd	2 nd bending	6855.98	2 nd bending	6820.82	-0.52%
4 th	2 nd torsional	7608.84	2 nd torsional	7547.12	-0.82%
5 th	1 st transversal bending	11 092.60	1 st transversal bending	11 042.50	-0.45%
6 th	3 rd torsional	11 883.34	1 st in-plane bending	11 533.59	–

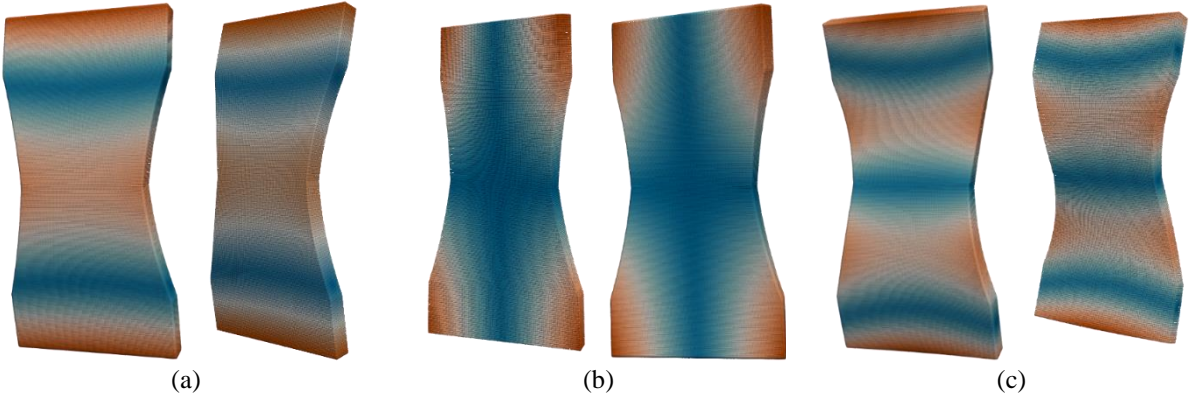


Fig. 7.3. Mode shapes of an undamaged specimen (left) and damaged specimen (right). a – the 1st bending mode; b – the 1st torsional mode; c – the 2nd bending mode.

8 CONCLUSIONS

This Thesis is an original research project that considered a novel approach to modal analysis in the peridynamic theory. A modal solver capable of solving peridynamic modal problems was implemented and optimized for a massively parallel computing environment. Further peridynamic modal simulations of models at nine different crack configurations were performed. Finite-element modal analyses were run for models at the same nine crack configurations. Then experimental test specimens were manufactured and tested to obtain both mechanical and modal properties. Next, the PD modal frequencies and mode shapes were verified against the FE results and validated against the experimental results. Lastly, an application of PD modal analysis was demonstrated by coupling it together with a fatigue damage simulation. Several conclusions can be drawn from this research.

1. The developed modal solver was optimized for and is capable of running in a massively parallel computing environment and solving peridynamic modal problems. Optimal parameter selection depends on the considered problem. However, optimization revealed several relations between the eigensolver, linear solver and preconditioner parameters and the simulation speed and memory use. These can be used as a starting point to determine optimal parameters in other cases.
2. The agreement between the peridynamic results and the FE results was excellent at all crack configurations. The differences in the computed modal frequencies ranged between 0.00 % and -4.00 %. The peridynamic modal frequencies were lower as the horizon increased. This behavior is explained by the increasing “surface effect”. Additionally, PD results also agreed well with the experimental results. The modal frequencies were within ± 3.2 % of the experimental results. Moreover, the PD frequency shift is similar to frequency shifts in FE and experimental analyses. The largest difference between the PD and the FE frequency shifts was -1.38 and 1.30 percentage points for T and S crack configurations respectively, but between the PD and the experimental frequency shifts -1.47 and 1.95 for T and S configurations respectively. The PD and the FE mode shapes agreed well and were in the same order at each crack configuration. The agreement between the PD and the experimental mode shapes was also good, furthermore, the change in the mode shapes from the introduced damage was similar in both analyses.
3. Two convergences – δm and δ – were considered. In the δm convergence study, results asymptotically approached a single value as the mesh density increased. The convergence is faster than linear, but slower than quadratic. Generally, the convergence order is between 1 and 2. Moreover, it was shown that the asymptotic range of convergence is reached with the 625 000-node model. Additionally, longer horizon results in lower computed frequencies, however, there are few exceptions in models with low mesh density. The δ -convergence plots were not asymptotic and showed that the difference between the non-local and the local solution does not shrink smoothly as the horizon decreases.

4. An example of a practical application of the current implementation of PD modal analysis was shown. The modal solver was coupled with a peridynamic fatigue damage simulation to demonstrate how the change in modal parameters due to fatigue damage can be assessed. First, the modal analysis was run. Next, 870 000 fatigue cycles were simulated. Lastly, modal analysis was run again. Mode shapes displayed no visible difference before and after the fatigue simulation, however, only qualitative assessment was done, but quantitative assessment is beyond the scope of this Thesis. The difference in modal frequencies for the same modes ranged between -2.91% to -0.45% . Showing that the damage created by a fatigue simulation can be measured using modal analysis. Such measurements can be applied in model validation, manufacturing quality assurance, and structural damage detection.